

Tensor network approach to two-dimensional Yang–Mills theories

Masafumi Fukuma¹, Daisuke Kadoh^{2,3}, and Nobuyuki Matsumoto^{4,*}

¹*Department of Physics, Kyoto University, Kyoto 606-8502, Japan*

²*Faculty of Sciences and Engineering, Doshisha University, Kyoto 610-0394, Japan*

³*Research and Educational Center for Natural Sciences, Keio University, Yokohama 223-8521, Japan*

⁴*RIKEN/BNL Research Center, Brookhaven National Laboratory, Upton, NY 11973, USA*

*E-mail: nobuyuki.matsumoto@riken.jp

Received August 6, 2021; Revised October 15, 2021; Accepted October 29, 2021; Published November 1, 2021

.....
 We propose a novel tensor network representation for two-dimensional Yang–Mills theories with arbitrary compact gauge groups. In this method, tensor indices are given directly by group elements with no direct use of the character expansion. We apply the tensor renormalization group method to this tensor network for $SU(2)$ and $SU(3)$, and find that the free energy density and the energy density are accurately evaluated. We also show that the singular value decomposition of a tensor has a group-theoretic structure and can be associated with the character expansion.

Subject Index A20, B01, B38, B64

1. Introduction

The tensor network (TN) method [1–5] is an attractive approach for studying many-body systems, because it is free from the sign problem in the first place,¹ and has the potential to precisely investigate critical phenomena in the large-volume limit. In field theory, the tensor renormalization group (TRG) method [3] and its variations [24–26] are widely used to study various models such as the Schwinger model [27–30], the Gross–Neveu and NJL models [31, 32], scalar field theories [33–36], the Yang–Mills and gauge–Higgs models [37, 38], the Wess–Zumino model [39], and other related models [40–42].

For gauge groups $U(1)$ [27–29, 40, 43] and $SU(2)$ [37, 38], character expansion was employed to represent the partition function with a tensor network. However, since character expansion becomes a demanding task for higher-rank gauge groups, it remains difficult to apply the TN method to $SU(N)$ gauge theory for $N \geq 3$ including quantum chromodynamics.

In this paper we propose a novel method for creating a tensor network for two-dimensional Yang–Mills theory with no direct use of character expansion. The Haar measure is discretized, and the group integration is replaced by a summation over K randomly generated configurations. Then, the plaquette is regarded as a rank-4 tensor whose index runs from 1 to K , and the set of plaquettes constitutes a tensor network. We test our method for $SU(2)$ and $SU(3)$ gauge groups, and find that the free energy density and the energy density agree very well with exact

¹Recently, significant progress has also been made in the Monte Carlo (MC) approach to the sign problem [6–23], giving rise to the hope that MC simulations can be performed at a reasonable computational cost. The two approaches (TN and MC) may play complementary roles in the future.

results. We also clarify the mathematical structure behind our method. In fact, the coefficients in the character expansion are approximately generated by our method.

The paper is organized as follows. In Sect. 2 we introduce our tensor network representation for two-dimensional Yang–Mills theories with arbitrary compact gauge groups G , and discuss its relation to the character expansion. In Sect. 3 we test our method for $G = SU(2)$ and $G = SU(3)$. Section 4 is devoted to a summary and discussion. The appendices provide some useful formulas in group theory.

2. Tensor network representations for two-dimensional Yang–Mills theories

In this section we introduce a new tensor network representation for two-dimensional Yang–Mills theories, and discuss its relation to character expansion. We exclusively consider pure Yang–Mills theory for simplicity. It is straightforward to extend our method to systems with interacting matter fields.

2.1 Method

We consider the Yang–Mills theory with a compact gauge group G on an infinite lattice $\Gamma \equiv \{n = (n_1, n_2) \mid n_\mu \in \mathbb{Z} (\mu = 1, 2)\}$. The lattice spacing a is set to $a = 1$ unless otherwise noted, and $\hat{\mu}$ is the unit vector in the μ direction.

Let $U_\mu(n)$ be the G -valued link field on links $(n, n + \hat{\mu})$. The lattice action (the Wilson action) is given by²

$$S = \frac{\beta}{N} \sum_{n \in \Gamma} \text{Re tr} [1 - U_P(n)], \tag{1}$$

where $U_P(n)$ is the plaquette field,

$$U_P(n) = U_1(n) U_2(n + \hat{1}) U_1^\dagger(n + \hat{2}) U_2^\dagger(n). \tag{2}$$

The partition function is defined as $Z = \int DU e^{-S}$, where $DU \equiv \prod_{n \in \Gamma} dU_1(n) dU_2(n)$ with dU the Haar measure of G . Note that the partition function Z can be written in the form of a tensor network with indices continuously taking values in G ,

$$Z = \mathfrak{Tr} \prod_{n \in \Gamma} \mathfrak{F}_{g(n)h(n)g'(n)h'(n)}, \tag{3}$$

where

$$\mathfrak{F}_{g_1 g_2 g_3 g_4} = e^{-(\beta/N) \text{Re tr} (1 - g_1 g_2 g_3^\dagger g_4^\dagger)} \tag{4}$$

and \mathfrak{Tr} stands for the group integrations for $g(n), h(n) \in G (n \in \Gamma)$ under a proper identification of indices.³

We now discretize the Haar measure dU to represent Z as a tensor network with indices in a finite range:

$$\int dU f(U) \approx \frac{1}{K} \sum_{i=1}^K f(U_i), \tag{5}$$

²We obtain the usual continuum action for $\beta = 2N/(ga)^2$ with $U_P(n) \simeq \exp(ia^2 F_{12}(n))$ in the naive continuum limit.

³We make the identifications $g'(n) = g(n + \hat{2})$ and $h'(n) = h(n - \hat{1})$.

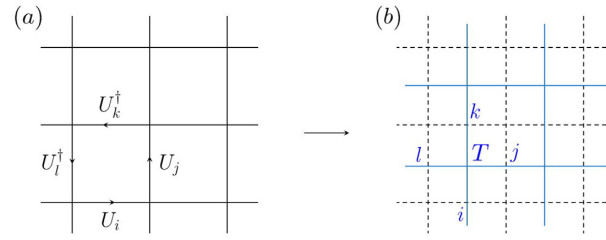


Fig. 1. Two-dimensional square lattice. (a) A plaquette variable consisting of U_i, U_j, U_k, U_l . (b) The corresponding tensor from Eq. (7) assigned to the center of the plaquette.

where $\mathring{G} = \{U_1, U_2, \dots, U_K\}$ consists of random points uniformly chosen from the group manifold. Applying Eq. (5) to the Haar measures in DU leads to

$$Z \approx \text{Tr} \prod_{n \in \Gamma} T_{i_n j_n i'_n j'_n}, \tag{6}$$

where

$$T_{ijkl} = \frac{1}{K^2} e^{-(\beta/N) \text{Re tr} (1 - U_i U_j U_k^\dagger U_l^\dagger)} \tag{7}$$

and Tr stands for the summation over $i_n, j_n = 1, 2, \dots, K$ for all $n \in \Gamma$ under the same identification of indices as above. As shown in Fig. 1, the tensor is assigned to each plaquette and has four indices corresponding to four links of the plaquette.

Since our method is based on the discrete approximation with finite K , we check the convergence of the right-hand side of Eq. (6) for large K in actual numerical computations.

In the tensor network in Eq. (6), a single set \mathring{G} is commonly used to discretize all the $U_\mu(n)$ -integrations. Actually, we can use a different set for each link. For example, tensors can be decomposed in different ways for even and odd sites [3], and we can use four different sets, $\mathring{G}_1, \mathring{G}_2, \mathring{G}_3,$ and \mathring{G}_4 , to discretize the integrations at the four links $U_i, U_j, U_k,$ and U_l in Fig. 1. We then have

$$Z \approx \text{Tr} \prod_{n \in \Gamma_e} T_{i_n j_n i'_n j'_n}^e \cdot \prod_{m \in \Gamma_o} T_{i_m j_m i'_m j'_m}^o, \tag{8}$$

with

$$T_{ijkl}^e \equiv \frac{1}{K^2} e^{-(\beta/N) \text{Re Tr} (1 - U_i^{(1)} U_j^{(2)} U_k^{(3)\dagger} U_l^{(4)\dagger})}, \tag{9}$$

$$T_{ijkl}^o \equiv \frac{1}{K^2} e^{-(\beta/N) \text{Re Tr} (1 - U_i^{(3)} U_j^{(4)} U_k^{(1)\dagger} U_l^{(2)\dagger})}, \tag{10}$$

where $U_i^{(a)} \in \mathring{G}_a$ ($a = 1, 2, 3, 4$) and $\Gamma_{e/o}$ is the set of even or odd sites, respectively. The introduction of four different sets significantly improves the precision of the results compared to a single set, as presented in Sect. 3.

Once the tensor network is obtained, any TRG method can be applied straightforwardly. In the Levin–Nave TRG, singular value decomposition (SVD) is employed to decompose the tensors. In general, the SVD of an $n \times n$ matrix M_{ij} is given by

$$M_{ij} = \sum_{a=1}^n \sigma_a U_{ia} V_{ja}^*, \tag{11}$$

where σ_a are singular values sorted as $\sigma_1 \geq \sigma_2 \geq \dots \geq \sigma_n \geq 0$, and U, V are unitary matrices. In our case, regarding T_{ijkl}^e (resp. T_{ijkl}^o) as a matrix with the column ij (resp. jk) and the row kl (resp. li), we have

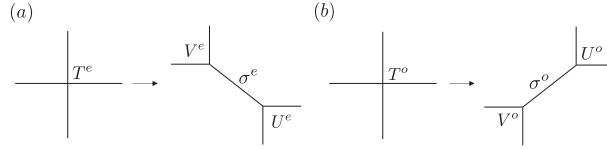


Fig. 2. The SVDs of an even tensor (a) and an odd tensor (b).

$$T_{ijkl}^e = \sum_{A=1}^{K^2} \sigma_A^e U_{ij,A}^e V_{kl,A}^{e*}, \tag{12}$$

$$T_{ijkl}^o = \sum_{A=1}^{K^2} \sigma_A^o U_{jk,A}^o V_{li,A}^{o*}. \tag{13}$$

Figure 2 shows these decompositions. We again arrive at the tensor network of the two-dimensional square lattice by defining the renormalized tensor $T^{(1)}$ with bond dimension D as

$$T_{A_1 A_2 A_3 A_4}^{(1)} = \sqrt{\sigma_{A_1}^e \sigma_{A_2}^o \sigma_{A_2}^e \sigma_{A_4}^o} \sum_{i,j,k,l=1}^D U_{ij,A_1}^e V_{jk,A_2}^{o*} V_{kl,A_3}^{e*} U_{li,A_4}^o. \tag{14}$$

The tensor network is repeatedly renormalized in this way.

Since the bond dimension of the initial tensors [Eqs. (9) and (10)] is K , the cost of the first SVD scales with $O(K^6)$. Once the tensors are renormalized, the bond dimension changes to D . The cost of the subsequent iterations then scales with $O(D^6)$.

2.2 Relation to the character expansion

To understand the group-theoretic structure of the SVD in the previous subsection, we consider the limit $K \rightarrow \infty$, i.e. the case where the tensor indices continuously take all the values in G . See Appendix A for the mathematical material necessary for the argument below.

Let R be an irreducible unitary representation of G with dimension d_R , and $D_R(U) = (D_{rs}^R(U)) (r, s = 1, 2, \dots, d_R)$ the representation matrix of U . Denoting the character of R by $\chi_R(U)$, the function $e^{-(\beta/N) \text{Re tr}(1-U)}$ can be expanded as

$$e^{-(\beta/N) \text{Re tr}(1-U)} = \sum_R d_R \lambda_R(\beta) \chi_R(U). \tag{15}$$

Here, and hereafter, \sum_R stands for the summation over the irreducible representations R . The coefficients $\lambda_R(\beta)$ are given by

$$\lambda_R(\beta) = \frac{1}{d_R} \int dU e^{-(\beta/N) \text{Re tr}(1-U)} \chi_R(U^{-1}), \tag{16}$$

as can be shown by using Eq. (A8).

We again consider the infinite-dimensional rank-4 tensor $\mathfrak{T}_{g_1 g_2 g_3 g_4}$ [see Eq. (4)]. By using Eq. (15), this can be written as $\sum_R d_R \lambda_R \chi_R(g_1 g_2 g_3^{-1} g_4^{-1})$ and decomposed in two ways:

$$\mathfrak{T}_{g_1 g_2 g_3 g_4} = \sum_{A=(R,r,s)} \mathfrak{U}_{(g_1, g_2), A}^e \lambda_R \mathfrak{W}_{(g_3, g_4), A}^{e*} = \sum_{A=(R,r,s)} \mathfrak{U}_{(g_2, g_3), A}^o \lambda_R \mathfrak{W}_{(g_4, g_1), A}^{o*}, \tag{17}$$

with

$$\mathfrak{U}_{(g_1, g_2), A}^e = \mathfrak{W}_{(g_2, g_1), A}^e = \mathfrak{U}_{(g_1, g_2^{-1}), A}^o = \mathfrak{W}_{(g_2, g_1^{-1}), A}^o \equiv \sqrt{d_R} D_{rs}^R(g_1 g_2). \tag{18}$$

The Peter–Weyl theorem (see Appendix A) states that the matrix $W_{g,A} \equiv \sqrt{d_R} D_{rs}^R(g)$ is unitary. Thus, together with the inequality $\lambda_R \geq 0$,⁴ we find that the decompositions in Eq. (17) are actually SVDs. Then, the new tensor $\mathfrak{T}^{(1)}$ [Eq. (14) with $D = \infty$] is calculated by following Eqs. (12)–(14) and is found to be⁵

$$\mathfrak{T}_{A_1 A_2 A_3 A_4}^{(1)} = \frac{\lambda_{R_1}^2}{d_{R_1}} \delta_{R_1 R_2 R_3 R_4} \delta_{s_1 s_2} \delta_{r_2 s_3} \delta_{r_3 r_4} \delta_{s_4 r_1}. \tag{19}$$

Once this expression is obtained, one can easily find that

$$Z = \sum_R \lambda_R(\beta)^V \tag{20}$$

by taking the whole contraction of the TN for Eq. (19) exactly, or using the TRG iterations without truncations (see Appendix C).

Recall that the TN representation [Eqs. (8)–(10)] is a discretization of Eqs. (3) and (4). Thus, our method approximately reproduces the tensor network that is obtained by the character expansion. Note that the singular values of the tensor $\mathfrak{T}_{g_1 g_2 g_3 g_4}$ have a degeneracy of d_R^2 for each R because both r and s in $W_{g,A} = \sqrt{d_R} D_{rs}^R(g)$ take d_R values. This means that the singular values σ_A of our tensor T_{ijkl} [Eqs. (12) and (13)] must have this degeneracy approximately. We actually find this approximate degeneracy in numerical calculations presented in the next section.

3. Numerical results

In this section we apply our method to the Yang–Mills theory with gauge group $G = SU(N)$ ($N = 2, 3$) on a periodic square lattice. We construct the tensor network with four different sets \hat{G}_a ($a = 1, 2, 3, 4$) of K random link variables [see the discussion after Eqs. (8)–(10)]. We evaluate the free energy density $f(\beta) \equiv (1/V) \ln Z(\beta)$ with the Levin–Nave TRG, and the energy density $e(\beta) \equiv -(\partial/\partial\beta)f(\beta)$ by taking numerical derivatives. Note that the estimates have statistical errors in addition to the systematic errors coming from the finiteness of K and bond dimension D . The statistical errors given below are obtained from five independent trials.

3.1 $SU(2)$

We first make a detailed analysis for $SU(2)$.

Figure 3 shows $f(\beta)$ for various volumes $V = L^2$ ($L = 4, 8, 16, 32, 64$) with β/V fixed to 0.01. The exact values are indicated by the gray dashed line. Figure 4 shows the errors relative to the exact values for the same calculation.

We see that the numerical results agree well with the exact values. We also see that as V (and thus β) is increased, larger K and D are required to decrease the systematic errors. Figures 5 and 6 show the K, D dependences of the free energy density at $V = 64^2$ ($\beta = 40.96$). We confirm that the numerical estimates approach the exact value in the limit $K \rightarrow \infty$ and $D \rightarrow \infty$.

⁴This can be proved by rewriting Eq. (16) in the form

$$e^\beta d_R \lambda_R = \int dU e^{(\beta/(2N))[\text{tr} U + \text{tr} U^{-1}]} \chi_R(U^{-1}) = \sum_{m,n=0}^{\infty} \left(\frac{\beta}{2N}\right)^{m+n} \frac{C_R^{(m,n)}}{m! n!}.$$

In fact, $C_R^{(m,n)} \equiv \int dU [\text{tr} U]^m [\text{tr} U^{-1}]^n \chi_R(U^{-1}) = \int dU [\chi_N(U)]^m [\chi_{\bar{N}}(U)]^n \chi_R(U^{-1})$ is the multiplicity of R in the product representation $N^{\otimes m} \otimes \bar{N}^{\otimes n}$, and thus is a nonnegative integer. (N and \bar{N} are the fundamental and anti-fundamental representations, respectively.)

⁵We use the symbol $\delta_{R_1 R_2 \dots R_k} \equiv \delta_{R_1 R_2} \delta_{R_2 R_3} \dots \delta_{R_{k-1} R_k}$.

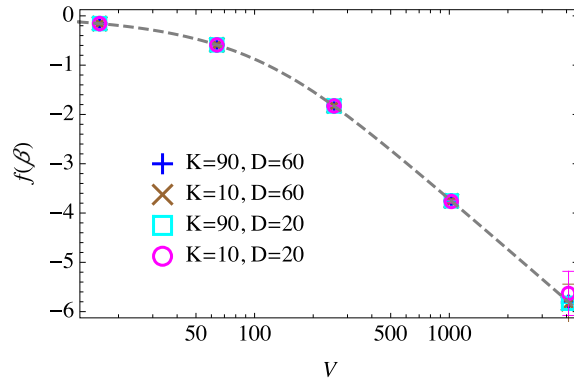


Fig. 3. Volume dependence of $f(\beta)$ with $\beta/V = 0.01$ for $SU(2)$. The exact values are expressed by the gray dashed line.

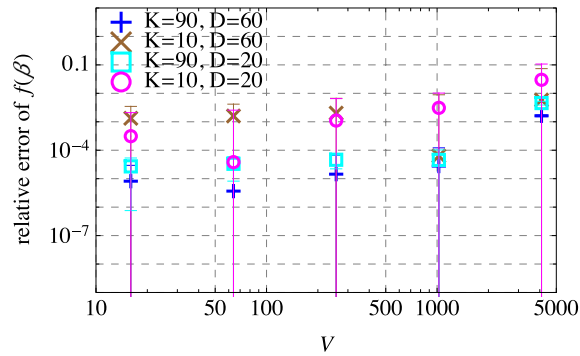


Fig. 4. Relative error of the free energy density, $|f(\beta) - f_{\text{exact}}(\beta)| / |f_{\text{exact}}(\beta)|$, against volume V with $\beta/V = 0.01$ for $SU(2)$.

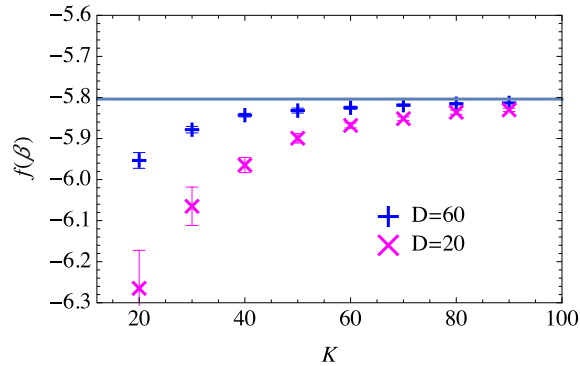


Fig. 5. K dependence of $f(\beta)$ with $\beta/V = 0.01$ and $V = 64^2$ ($\beta = 40.96$) for $SU(2)$.

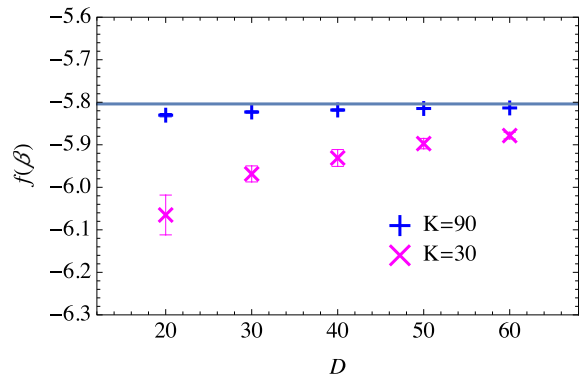


Fig. 6. D dependence of $f(\beta)$ with $\beta/V = 0.01$ and $V = 64^2$ ($\beta = 40.96$) for $SU(2)$.

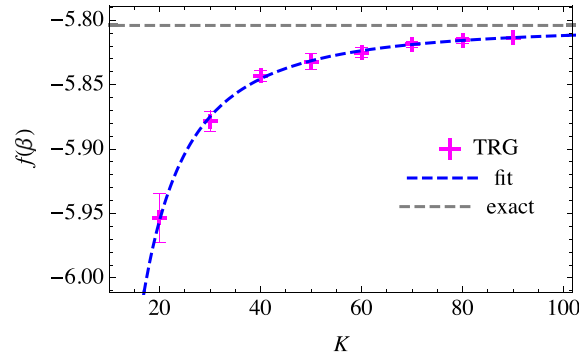


Fig. 7. χ^2 fit of the free energy densities $f(\beta)$ for various K with $\beta/V = 0.01$, $V = 64^2$, and $D = 60$ for $SU(2)$.

Table 1. Results of the χ^2 fit in Eq. (21) for $SU(2)$.

	(exact)	μ	α	p	χ^2/DOF
$f(\beta)$	-5.8040	$-5.8045^{+0.0040}_{-0.0029}$	-43^{+26}_{-60}	$1.88^{+0.27}_{-0.28}$	0.13
$e(\beta)$	0.03639	$0.03655^{+0.00029}_{-0.00052}$	5^{+24}_{-5}	$2.00^{+0.49}_{-0.53}$	0.11

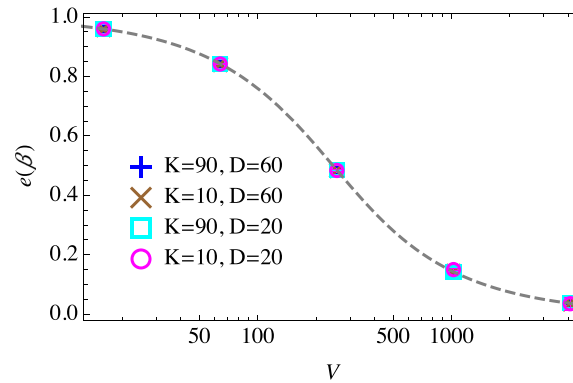


Fig. 8. Volume dependence of $e(\beta)$ with $\beta/V = 0.01$ for $SU(2)$.

Having obtained the estimates for several values of K , we can make use of extrapolation to obtain a better estimate. Figure 7 shows the χ^2 fit to the obtained data for $D = 60$ with the scaling ansatz $g(K) \equiv \mu + \alpha K^{-p}$. Here, the fitting parameters α , μ , and p are determined by minimizing the cost function

$$\chi^2(\mu, \alpha, p) \equiv \sum_{K=20,30,\dots,90} \frac{[f(\beta; K) - g(K)]^2}{[\delta f(\beta; K)]^2}, \quad (21)$$

where $f(\beta; K)$ is the value obtained for each K , and $\delta f(\beta; K)$ the statistical error. The value of μ is then used as the final estimate of $f(\beta)$.

The results of the fitting are summarized in Table 1. We obtain $\mu = -5.8045^{+0.0040}_{-0.0029}$, which agrees well with the exact value $f_{\text{exact}}(\beta) = -5.8040$. Since the estimate without extrapolation is given by $f(\beta; K = 90) \approx -5.81365 \pm 0.00032$, we see that the extrapolation significantly improves the accuracy.

We now show the results for the energy density $e(\beta)$. In Fig. 8, we plot the estimates of $e(\beta)$ for various V with $\beta/V = 0.01$ fixed, and in Fig. 9 the errors relative to the exact values. We

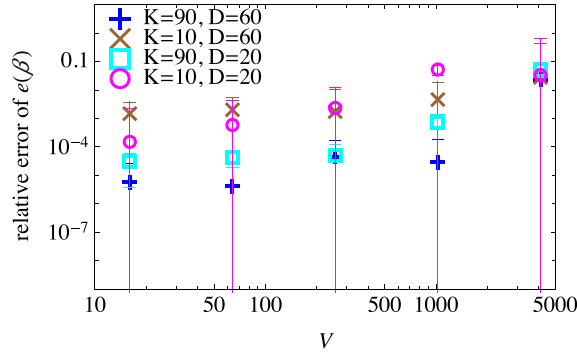


Fig. 9. Relative error of the energy density, $|e(\beta) - e_{\text{exact}}(\beta)| / |e_{\text{exact}}(\beta)|$, with $\beta/V = 0.01$ for $SU(2)$.

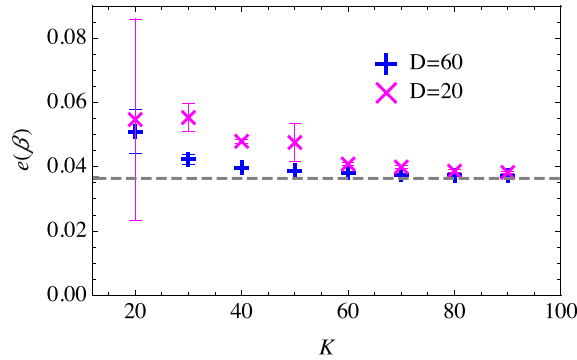


Fig. 10. K dependence of $e(\beta)$ with $\beta/V = 0.01$ for $SU(2)$.

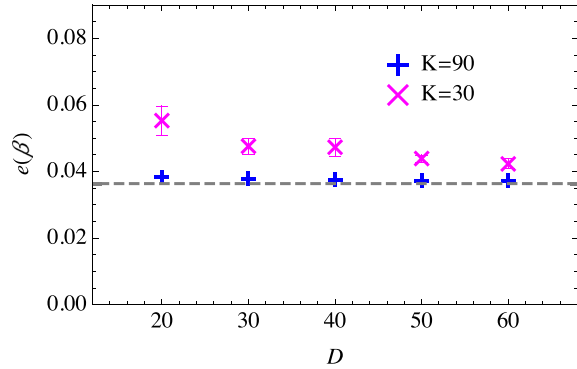


Fig. 11. D dependence of $e(\beta)$ with $\beta/V = 0.01$ for $SU(2)$.

again see good agreements, suggesting the effectiveness of our method. In Figs. 10 and 11, the K and D dependences are shown for $V = 64^2$ ($\beta = 40.96$), from which we again confirm that the numerical estimates approach the exact value in the limit $K \rightarrow \infty$ and $D \rightarrow \infty$.

We can make use of extrapolation to improve the accuracy. Figure 12 shows the χ^2 fit to the data obtained with the cost function in Eq. (21) with $f(\beta)$ replaced by $e(\beta)$. The results of the fitting are also given in Table 1.

Figure 13 shows the singular values σ_A of the initial tensor for $\beta = 2$ with $K = 90$.

For $SU(2)$, λ_R in Eq. (15) takes the following form (see Appendix B):

$$\lambda_{R=n}(\beta) = \frac{2}{\beta} e^{-\beta} I_n(\beta). \tag{22}$$

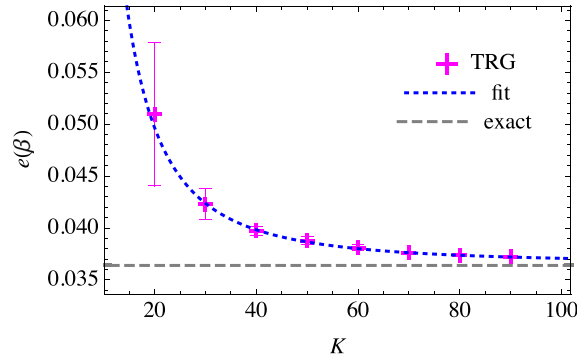


Fig. 12. Fitting of the energy densities $e(\beta)$ for various K with $\beta/V = 0.01$, $V = 64^2$, and $D = 60$ for $SU(2)$.

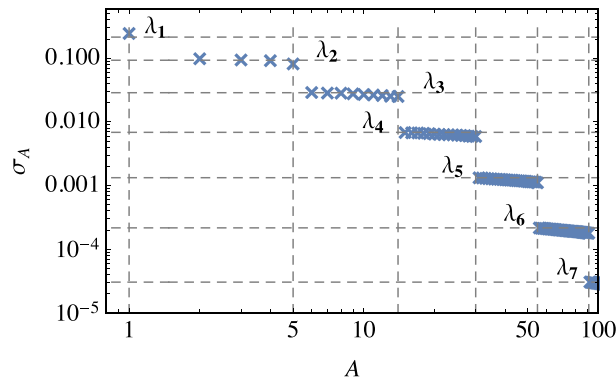


Fig. 13. Singular values σ_A of the initial tensors $T^{(e)}$ [Eq. (9)] with $\beta = 2$ and $K = 90$ for $SU(2)$. The horizontal lines indicate the exact values of $\lambda_R(\beta = 2)$, and the vertical lines the points at which the exact values change discontinuously.

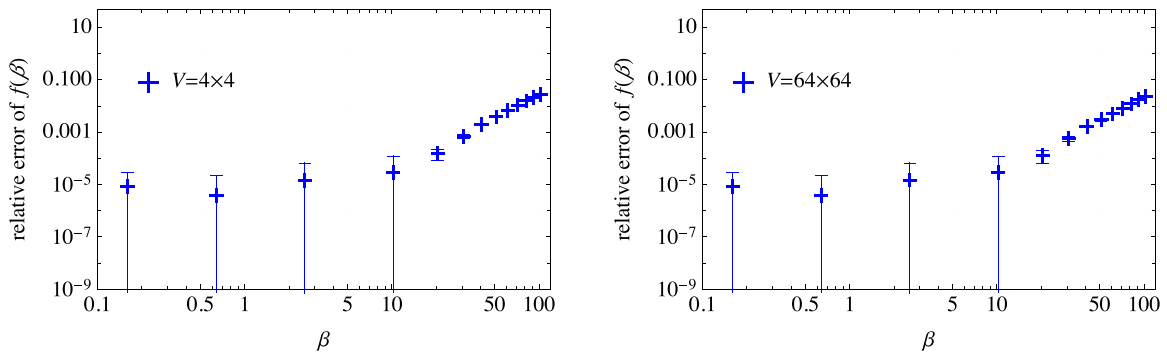


Fig. 14. Relative errors of $f(\beta)$ for varying β with fixed volumes $V = 4^2$ (left) and $V = 64^2$ (right) for $SU(2)$. We set $K = 90$ and $D = 60$. The relative error increases for large β in a manner almost independent of the volume.

Here, \mathbf{n} is the n -dimensional irreducible representation of $SU(2)$, and $I_n(z)$ is the modified Bessel function of the first kind. According to the discussion in Sect. 2.2, there will be $d_R^2 = n^2$ degenerate singular values in the limit $K \rightarrow \infty$ for each representation $R = \mathbf{n}$. In the figure, we clearly observe this degeneracy even for finite K ($K = 90$ here).

The accuracy of our method reduces at weak couplings (at large β). Figure 14 shows that the reduction mainly depends on β and is almost independent of the volume. The increasing

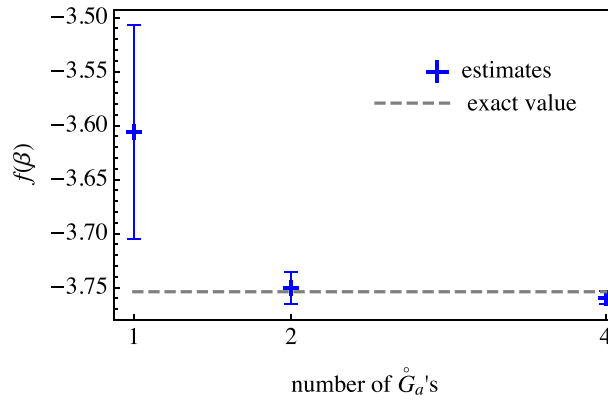


Fig. 15. Dependence of the estimate of $f(\beta)$ on the number of \hat{G}_a ($\beta/V = 0.04$, $V = 16^2$, $K = 20$, $D = 20$) for $SU(2)$. The statistical errors decrease as the number increases.

inaccuracy at large β can be attributed to two facts. One is that the singular values $\sigma_A(\beta)$ [approximating the character expansion coefficients $\lambda_R(\beta)$] become degenerate at large β , which requires a larger bond dimension D . This behavior should appear commonly in any methods that have a similarity to the character expansion. The second is that the integrand of the partition function has a sharp peak in the configuration space at large β , for which our uniform sampling becomes less effective. The appearance of this issue is unavoidable at this stage for tensor networks constructed with a sampling method such as the Gaussian quadrature or the random sampling we employed. The improvement in this direction is beyond the scope of the present paper and will be left for future work. The volume independence may be simply understood by the fact that the free energies at different volumes are estimated with the same initial tensor if other parameters are the same.

Finally, Fig. 15 shows the dependence of the estimate of $f(\beta)$ on the number of \hat{G}_a with $\beta/V = 0.04$, $V = 16^2$, $D = 20$, from which we see that the statistical errors decrease as the number increases. This behavior can be understood as follows. We first note that group elements enter the tensor only in the form of the product of two elements, $U_i U_j$, as can be seen from Eq. (17). We also note that a better approximation is achieved when the set of K^2 elements $\{U_i U_j\}$ ($i, j = 1, \dots, K$) is closer to the uniform distribution on G . As the number of \hat{G}_a increases, the set $\{U_i U_j\}$ gets more randomly distributed on G , which leads to a better estimate of observables with smaller statistical errors.

3.2 $SU(3)$

We make a similar analysis for $SU(3)$ with $\beta/V = 0.005$, $V = 64^2$, and $D = 90$. The irreducible representations R of $SU(3)$ are labeled by two nonnegative integers, $R = [q_1, q_2]$ (see Appendix B), for which the dimension is given by $d_R = (q_1 + 1)(q_2 + 1)(q_1 + q_2 + 2)/2$. The coefficients $\lambda_R(\beta)$ are given by the formula in Eq. (B2). One can show that they are ordered as⁶

$$\lambda_1 > \lambda_3 = \lambda_{\bar{3}} > \lambda_8 > \lambda_6 = \lambda_{\bar{6}} > \lambda_{15} = \lambda_{\bar{15}} > \lambda_{10} = \lambda_{\bar{10}} > \dots \quad (23)$$

⁶We write the irreducible representations $R = [q_1, q_2]$ (see Appendix B) as

$$\begin{aligned} [0, 0] &= \mathbf{1}, & [1, 0] &= \mathbf{3}, & [0, 1] &= \bar{\mathbf{3}}, & [1, 1] &= \mathbf{8}, & [2, 0] &= \mathbf{6}, & [0, 2] &= \bar{\mathbf{6}}, \\ [2, 1] &= \mathbf{15}, & [1, 2] &= \bar{\mathbf{15}}, & [3, 0] &= \mathbf{10}, & [0, 3] &= \bar{\mathbf{10}}, & \dots & & & \end{aligned}$$

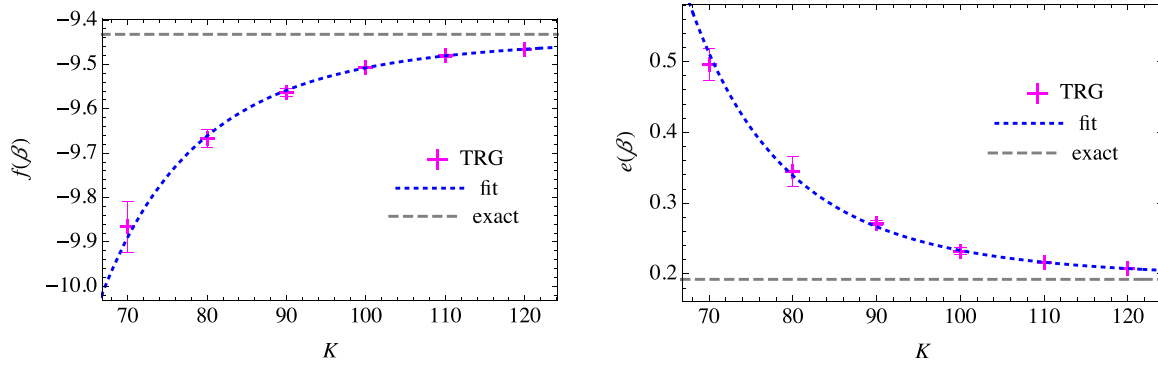


Fig. 16. K dependences of $f(\beta)$ (left panel) and $e(\beta)$ (right panel) with $\beta/V = 0.005$, $V = 64^2$, and $D = 90$ for $SU(3)$.

Table 2. Results of the χ^2 fit for $SU(3)$.

	(exact)	μ	α	p	χ^2/DOF
$f(\beta)$	-9.4323	$-9.4400^{+0.0019}_{-0.0043}$	$-0.3^{+0.2}_{-1.7} \times 10^{10}$	$5.31^{+0.44}_{-0.01}$	0.21
$e(\beta)$	0.1923	$0.1941^{+0.0017}_{-0.0008}$	$2.2^{+5.6}_{-1.6} \times 10^{10}$	$5.88^{+0.29}_{-0.01}$	1.18

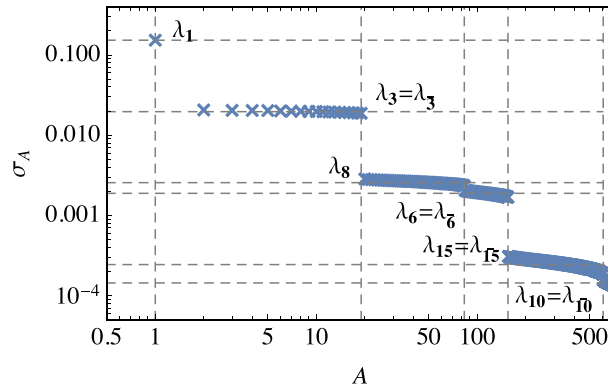


Fig. 17. Singular values σ_A of the initial tensors $T^{(e)}$ [Eq. (9)] with $\beta = 2$ and $K = 120$ for $SU(3)$. The horizontal lines indicate the exact values of $\lambda_R(\beta = 2)$, and the vertical lines the points at which the exact values change discontinuously.

In Fig. 16 we plot the free energy densities $f(\beta)$ and the energy densities $e(\beta)$ against various values of K . We make the χ^2 fit to the data obtained at $K = 70, 80, \dots, 120$, again with the scaling ansatz $g(K) \equiv \mu + \alpha K^{-p}$. A similar analysis is performed for $e(\beta)$. The results of the fitting are summarized in Table 2.

For the free energy density $f(\beta)$, we obtain the estimate $\mu = -9.4400^{+0.0019}_{-0.0043}$, which agrees well with the exact value $f_{\text{exact}}(\beta) = -9.4323$. For the energy density $e(\beta)$, we obtain the estimate $\mu = 0.1941^{+0.0017}_{-0.0008}$, which also agrees well with the exact value $e_{\text{exact}}(\beta) = 0.1923$. These good agreements show that our method also works for $SU(3)$.

The singular values of the initial tensor also agree with the character expansion coefficients $\lambda_R(\beta)$ for $SU(3)$. Figure 17 shows the singular values σ_A for $\beta = 2$ with $K = 120$.

We see that the coefficients are reproduced well with the correct degeneracies, reconfirming the group-theoretical structure discussed in Sect. 2.2.

4. Summary and discussion

We have proposed a novel tensor network representation for two-dimensional Yang–Mills theories with arbitrary compact gauge groups, which makes no direct use of the character expansion. The numerical results for $SU(2)$ and $SU(3)$ gauge groups show that our method works properly. Although this paper focuses on pure Yang–Mills theories, it is straightforward to include the dynamical degrees of freedom of fermions and scalar fields into the tensor.

As a future project, it will be important to investigate whether the precision is improved by applying other renormalization algorithms to our tensor network, such as the higher-order tensor renormalization group. It will also be interesting to develop a method to optimally choose group elements from the group manifold as the Gauss–Hermite quadrature for a field space with flat geometry. The extension of the framework to higher-dimensional Yang–Mills theories should also be one of the next steps to be considered. A study in this direction is now in progress and will be reported elsewhere.

Acknowledgements

This work was partially supported by JSPS KAKENHI (Grant Numbers 18J22698, 19K03853, 20H01900) and by SPIRITS (Supporting Program for Interaction-based Initiative Team Studies) of Kyoto University (PI: M.F.). D.K. would like to thank David C.-J. Lin for encouragement, and the members of NCTS in National Tsing-Hua University for their hospitality. N.M. is supported by the Special Postdoctoral Researchers Program of RIKEN.

Funding

Open Access funding: SCOAP³.

Appendix A. Mathematical formulas

In this appendix we summarize useful formulas for integration over a compact group G .

For a unitary representation R (not necessarily irreducible) with dimension d_R , we denote the representation matrix of $U \in G$ by $D_R(U) = (D_{rs}^R(U))$ ($r, s = 1, \dots, d_R$) and the character by $\chi_R(U) = \text{tr} D_R(U)$. Note that $\chi_R(1) = d_R$. Hereafter we use the term “representation” as meaning “representation class,” and fix a representative R for each representation class. Note that for a unitary representation, we have $D_{rs}^R(U^{-1}) = [D_{sr}^R(U)]^*$ and $\chi_R(U^{-1}) = [\chi_R(U)]^*$.

We introduce the Haar measure dU , which is two-side invariant and normalized:

$$\int dU f(g_1 U g_2) = \int dU f(U) \quad (\forall g_1, g_2 \in G), \quad (\text{A1})$$

$$\int dU f(U^{-1}) = \int dU f(U), \quad (\text{A2})$$

$$\int dU 1 = 1. \quad (\text{A3})$$

We also introduce the invariant delta function $\delta(U, V)$ associated with the Haar measure:

$$\int dU \delta(U, V) f(U) = f(V), \quad (\text{A4})$$

$$\delta(g_1 U g_2, g_1 V g_2) = \delta(U, V) \quad (\forall g_1, g_2 \in G), \quad (\text{A5})$$

$$\delta(U^{-1}, V^{-1}) = \delta(U, V). \quad (\text{A6})$$

We write the set of irreducible unitary representations by $\text{Irrep} = \{R : \text{irreducible}\}$. Then, we have the following formula for $R_1, R_2 \in \text{Irrep}$:⁷

$$\int dU D_{r_1 s_1}^{R_1}(U) D_{r_2 s_2}^{R_2}(U^{-1}) = \frac{\delta_{R_1 R_2}}{d_{R_1}} \delta_{r_1 s_2} \delta_{s_1 r_2}, \tag{A7}$$

from which we readily obtain the formulas for the integration of characters,

$$\int dU \chi_{R_1}(g_1 U) \chi_{R_2}(U^{-1} g_2) = \frac{\delta_{R_1 R_2}}{d_{R_1}} \chi_{R_1}(g_1 g_2), \tag{A8}$$

$$\int dU \chi_R(g_1 U g_2 U^{-1}) = \frac{1}{d_R} \chi_R(g_1) \chi_R(g_2). \tag{A9}$$

The characters of irreducible representations $\{\chi_R(U)\}$ ($R \in \text{Irrep}$) form a linear basis of the set of class functions $\{f(U)\}$ that satisfy $f(gUg^{-1}) = f(U)$ ($\forall g \in G$). In particular, as can be easily proved, $\delta(U, 1)$ is expanded as $\sum_{R \in \text{Irrep}} d_R \chi_R(U)$, and thus we have

$$\delta(U, V) = \sum_{R \in \text{Irrep}} d_R \chi_R(UV^{-1}) = \sum_{R \in \text{Irrep}} d_R \chi_R(VU^{-1}). \tag{A10}$$

From this equation readily follows the Peter–Weyl theorem, which states that the infinite-dimensional matrix

$$W_{U,A} \equiv \sqrt{d_R} D_{rs}^R(U) \quad [A = (R, r, s)] \tag{A11}$$

is unitary:

$$\int dU W_{U,A}^* W_{U,A'} = \delta_{AA'}, \quad \sum_A W_{U,A} W_{U',A}^* = \delta(U, U'), \tag{A12}$$

with $\delta_{AA'} \equiv \delta_{RR'} \delta_{rr'} \delta_{ss'}$ and $\sum_A \equiv \sum_{R \in \text{Irrep}} \sum_{r=1}^{d_R} \sum_{s=1}^{d_R}$.

Appendix B. $\lambda_R(\beta)$ for $G = SU(N)$

For $G = SU(N)$, the irreducible representation $R = [q_1, \dots, q_{N-1}]$ ($q_i \in \mathbb{Z}_{\geq 0}$: Dynkin labels) can be labeled by a Young diagram $Y = (f_1, f_2, \dots, f_{N-1})$ ($f_1 \geq f_2 \geq \dots \geq f_{N-1} \geq 0$) with the relations $f_i \equiv \sum_{j=i}^{N-1} q_j$ (see Fig. B1). The dimension d_R is given by

$$d_R = \Delta(\ell_1, \ell_2, \dots, \ell_{N-1}, \ell_N) / \Delta(N-1, N-2, \dots, 1, 0), \tag{B1}$$

where $\ell_i \equiv f_i + N - i$ with $f_N \equiv 0$ and $\Delta(x_1, \dots, x_N) \equiv \prod_{i < j} (x_i - x_j)$. One can show that the coefficients $\lambda_R(\beta)$ can be expressed as (see, e.g., Ref. [44])

$$\lambda_R(\beta) = \frac{e^{-\beta}}{d_R} \sum_{Q \in \mathbb{Z}} \det[I_{f_j+i-j+Q}(\beta/N)] \quad [G = SU(N)], \tag{B2}$$

where $I_n(z)$ are the modified Bessel functions of the first kind.

For $G = SU(2)$, the irreducible representation $R = [q]$ corresponds to the spin $j = q/2$ representation with $d_R = q + 1 = 2j + 1$, for which the infinite series in Eq. (B2) can be summed to a simple form,

$$\lambda_R(\beta) = (2/\beta) e^{-\beta} I_{2j+1}(\beta) \quad [G = SU(2)]. \tag{B3}$$

Thus, the free energy density and the energy density can be expressed as

$$f(\beta) = \frac{1}{V} \log \left[\sum_{n=1}^{\infty} \left(\frac{2}{\beta} e^{-\beta} I_n(\beta) \right)^V \right], \tag{B4}$$

⁷From this equation, one can show the formula

$$\int dU D_{r_1 s_1}^{R_1}(g_1 U) D_{r_2 s_2}^{R_2}(U^{-1} g_2) = \int dU D_{r_1 s_1}^{R_1}(g_1 U^{-1}) D_{r_2 s_2}^{R_2}(U g_2) = \frac{\delta_{R_1 R_2}}{d_{R_1}} \delta_{s_1 r_2} D_{r_1 s_2}^{R_1}(g_1 g_2).$$

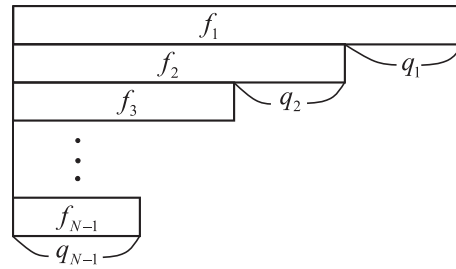


Fig. B1. Young diagram for $R = [q_1, \dots, q_{N-1}]$.

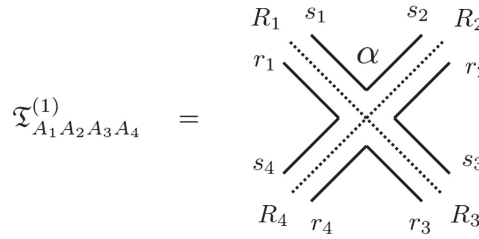


Fig. C1. Graphical representation of $\mathfrak{T}_{A_1 A_2 A_3 A_4}^{(1)}$.

$$e(\beta) = - \frac{\sum_{n=1}^{\infty} I_n^{V-1}(\beta) [(I_{n+1}(\beta) + I_{n-1}(\beta))/2 - I_n(\beta)/\beta]}{\sum_{n=1}^{\infty} I_n^V(\beta)} + 1. \tag{B5}$$

Appendix C. Tensor network derivation of the exact partition function

The well-known formula in Eq. (20) can be easily derived from the TN representation of the partition function with the infinite-dimensional tensor, Eq. (19):

$$\mathfrak{T}_{A_1 A_2 A_3 A_4}^{(1)} = \alpha_1 \delta_{R_1 R_2 R_3 R_4} \delta_{s_1 s_2} \delta_{r_2 s_3} \delta_{r_3 r_4} \delta_{s_4 r_1}. \tag{C1}$$

Here, $A_i = (R_i, r_i, s_i)$, $\delta_{R_1 R_2 \dots R_m} = \delta_{R_1 R_2} \delta_{R_2 R_3} \dots \delta_{R_{m-1} R_m}$, and $\alpha_n \equiv \lambda_R^{2n} / d_R$ ($n = 1, 2, \dots$) are factors located at vertices. Figure C1 shows a graphical representation of $\mathfrak{T}^{(1)}$.

It is straightforward to evaluate the value of Z as shown in Fig. C2. Figure C2(b) is obtained from Fig. C2(a) where α_1 is replaced by $\alpha_1 d_R = \lambda_R^2$ because d_R is provided from the inner loop. The final expression is immediately obtained because the remaining tensors in Fig. C2(b) are diagonal with respect to the R indices [38].

Instead, we can use the TRG iterations to evaluate Z . Omitting the tensor indices, we write

$$\mathfrak{T}^{(1)} = \dots \tag{C2}$$

Then, we decompose $\mathfrak{T}^{(1)}$ in two ways as

$$\mathfrak{T}^{(1)} = \dots = \dots \tag{C3}$$

$$Z = \text{(a)} = \text{(b)} = \sum_R \lambda_R(\beta)^V$$

Fig. C2. The TN representation of the partition function with the infinite-dimensional tensor.

where rank-3 tensors are defined in a manner similar to Eq. (C1). These decompositions correspond to the SVDs given in Fig. 2. With these rank-3 tensors, we construct the second tensor as

$$\mathfrak{T}^{(2)} = \text{(diamond with } \sqrt{\alpha_1} \text{ legs)} = \text{(cross with } \alpha_2 \text{ center)} \quad (C4)$$

Note that we have not made any truncation. Repeating this procedure, we have the n th tensor

$$\mathfrak{T}^{(n)} = \text{(cross with } \alpha_n \text{ center)} \quad (C5)$$

from which the partition function Z with volume $V = 2^n$ is calculated as

$$Z = \text{(torus with } \alpha_n \text{ loops)} = \sum_R \lambda_R(\beta)^V \quad (C6)$$

References

- [1] H. Niggemann, A. Klumper, and J. Zittartz, *Z. Phys. B* **104**, 103 (1997) [[arXiv:cond-mat/9702178](#)] [[Search inSPIRE](#)].
- [2] F. Verstraete and J. I. Cirac, [[arXiv:cond-mat/0407066](#)] [[Search inSPIRE](#)].
- [3] M. Levin and C. P. Nave, *Phys. Rev. Lett.* **99**, 120601 (2007) [[arXiv:cond-mat/0611687](#)] [[Search inSPIRE](#)].
- [4] Z. Y. Xie, H. C. Jiang, Q. N. Chen, Z. Y. Weng, and T. Xiang, *Phys. Rev. Lett.* **103**, 160601 (2009) [[arXiv:0809.0182](#) [cond-mat.str-el]] [[Search inSPIRE](#)].
- [5] Z. C. Gu, F. Verstraete, and X. G. Wen, [arXiv:1004.2563](#) [cond-mat.str-el] [[Search inSPIRE](#)].
- [6] G. Parisi, *Phys. Lett. B* **131**, 393 (1983).
- [7] J. R. Klauder, *Phys. Rev. A* **29**, 2036 (1984).
- [8] G. Aarts, F. A. James, E. Seiler, and I. O. Stamatescu, *Phys. Lett. B* **687**, 154 (2010) [[arXiv:0912.0617](#) [hep-lat]] [[Search inSPIRE](#)].
- [9] J. Nishimura and S. Shimasaki, *Phys. Rev. D* **92**, 011501 (2015) [[arXiv:1504.08359](#) [hep-lat]] [[Search inSPIRE](#)].
- [10] E. Witten, Contribution to: Chern-Simons Gauge Theory: 20 years after, *AMS/IP Stud. Adv. Math* **50**, 347 (2011) [[arXiv:1001.2933](#) [hep-th]] [[Search inSPIRE](#)].

- [11] M. Cristoforetti, F. Di Renzo, and L. Scorzato, Phys. Rev. D **86**, 074506 (2012) [[arXiv:1205.3996](#)] [[hep-lat](#)] [[Search inSPIRE](#)].
- [12] M. Cristoforetti, F. Di Renzo, A. Mukherjee, and L. Scorzato, Phys. Rev. D **88**, 051501(R) (2013) [[arXiv:1303.7204](#)] [[hep-lat](#)] [[Search inSPIRE](#)].
- [13] H. Fujii, D. Honda, M. Kato, Y. Kikukawa, S. Komatsu, and T. Sano, J. High Energy Phys. **1310**, 147 (2013) [[arXiv:1309.4371](#)] [[hep-lat](#)] [[Search inSPIRE](#)].
- [14] A. Alexandru, G. Başar, P. F. Bedaque, G. W. Ridgway, and N. C. Warrington, J. High Energy Phys. **1605**, **053** (2016) [[arXiv:1512.08764](#)] [[hep-lat](#)] [[Search inSPIRE](#)].
- [15] M. Fukuma and N. Umeda, Prog. Theor. Exp. Phys. **2017**, 073B01 (2017) [[arXiv:1703.00861](#)] [[hep-lat](#)] [[Search inSPIRE](#)].
- [16] A. Alexandru, G. Başar, P. F. Bedaque, and N. C. Warrington, Phys. Rev. D **96**, 034513 (2017) [[arXiv:1703.02414](#)] [[hep-lat](#)] [[Search inSPIRE](#)].
- [17] M. Fukuma, N. Matsumoto, and N. Umeda, Phys. Rev. D **100**, 114510 (2019) [[arXiv:1906.04243](#)] [[cond-mat.str-el](#)] [[Search inSPIRE](#)].
- [18] M. Fukuma, N. Matsumoto, and N. Umeda, [arXiv:1912.13303](#) [[hep-lat](#)] [[Search inSPIRE](#)].
- [19] M. Fukuma and N. Matsumoto, Prog. Theor. Exp. Phys. **2021**, (2021) [[arXiv:2012.08468](#)] [[hep-lat](#)] [[Search inSPIRE](#)].
- [20] M. Fukuma, N. Matsumoto, and Y. Namekawa, Prog. Theor. Exp. Phys., [arXiv:2107.06858](#) [[hep-lat](#)] [[Search inSPIRE](#)].
- [21] Y. Mori, K. Kashiwa, and A. Ohnishi, Phys. Rev. D **96**, 111501 (2017) [[arXiv:1705.05605](#)] [[hep-lat](#)] [[Search inSPIRE](#)].
- [22] Y. Mori, K. Kashiwa, and A. Ohnishi, Prog. Theor. Exp. Phys. **2018**, 023B04 (2018) [[arXiv:1709.03208](#)] [[hep-lat](#)] [[Search inSPIRE](#)].
- [23] A. Alexandru, P. F. Bedaque, H. Lamm, and S. Lawrence, Phys. Rev. D **97**, 094510 (2018) [[arXiv:1804.00697](#)] [[hep-lat](#)] [[Search inSPIRE](#)].
- [24] Z. Y. Xie, J. Chen, M. P. Qin, J. W. Zhu, L. P. Yang, and T. Xiang, Phys. Rev. B **86**, 045139 (2012) [[arXiv:1201.1144](#)] [[cond-mat.stat-mech](#)] [[Search inSPIRE](#)].
- [25] D. Adachi, T. Okubo, and S. Todo, Phys. Rev. B **102**, 054432 (2020) [[arXiv:1906.02007](#)] [[cond-mat.stat-mech](#)] [[Search inSPIRE](#)].
- [26] D. Kadoh and K. Nakayama, [arXiv:1912.02414](#) [[hep-lat](#)] [[Search inSPIRE](#)].
- [27] Y. Shimizu and Y. Kuramashi, Phys. Rev. D **90**, 014508 (2014) [[arXiv:1403.0642](#)] [[hep-lat](#)] [[Search inSPIRE](#)].
- [28] Y. Shimizu and Y. Kuramashi, Phys. Rev. D **90**, 074503 (2014) [[arXiv:1408.0897](#)] [[hep-lat](#)] [[Search inSPIRE](#)].
- [29] Y. Shimizu and Y. Kuramashi, Phys. Rev. D **97**, 034502 (2018) [[arXiv:1712.07808](#)] [[hep-lat](#)] [[Search inSPIRE](#)].
- [30] N. Butt, S. Catterall, Y. Meurice, R. Sakai, and J. Unmuth-Yockey, Phys. Rev. D **101**, 094509 (2020) [[arXiv:1911.01285](#)] [[hep-lat](#)] [[Search inSPIRE](#)].
- [31] S. Takeda and Y. Yoshimura, Prog. Theor. Exp. Phys. **2015**, 043B01 (2015) [[arXiv:1412.7855](#)] [[hep-lat](#)] [[Search inSPIRE](#)].
- [32] S. Akiyama, Y. Kuramashi, T. Yamashita, and Y. Yoshimura, J. High Energy Phys. **01**, 121 (2021) [[arXiv:2009.11583](#)] [[hep-lat](#)] [[Search inSPIRE](#)].
- [33] D. Kadoh, Y. Kuramashi, Y. Nakamura, R. Sakai, S. Takeda, and Y. Yoshimura, J. High Energy Phys. **05**, 184 (2019) [[arXiv:1811.12376](#)] [[hep-lat](#)] [[Search inSPIRE](#)].
- [34] D. Kadoh, Y. Kuramashi, Y. Nakamura, R. Sakai, S. Takeda, and Y. Yoshimura, J. High Energy Phys. **02**, 161 (2020) [[arXiv:1912.13092](#)] [[hep-lat](#)] [[Search inSPIRE](#)].
- [35] S. Akiyama, D. Kadoh, Y. Kuramashi, T. Yamashita, and Y. Yoshimura, J. High Energy Phys. **09**, 177 (2020) [[arXiv:2005.04645](#)] [[hep-lat](#)] [[Search inSPIRE](#)].
- [36] S. Akiyama, Y. Kuramashi, and Y. Yoshimura, [arXiv:2101.06953](#) [[hep-lat](#)] [[Search inSPIRE](#)].
- [37] M. Asaduzzaman, S. Catterall, and J. Unmuth-Yockey, Phys. Rev. D **102**, 054510 (2020) [[arXiv:1905.13061](#)] [[hep-lat](#)] [[Search inSPIRE](#)].
- [38] A. Bazavov, S. Catterall, R. G. Jha, and J. Unmuth-Yockey, Phys. Rev. D **99**, 114507 (2019) [[arXiv:1901.11443](#)] [[hep-lat](#)] [[Search inSPIRE](#)].
- [39] D. Kadoh, Y. Kuramashi, Y. Nakamura, R. Sakai, S. Takeda, and Y. Yoshimura, J. High Energy Phys. **03**, 141 (2018) [[arXiv:1801.04183](#)] [[hep-lat](#)] [[Search inSPIRE](#)].

- [40] H. Kawauchi and S. Takeda, Phys. Rev. D **93**, 114503 (2016) [[arXiv:1603.09455](#) [hep-lat]] [[Search inSPIRE](#)].
- [41] S. Akiyama and D. Kadoh, [arXiv:2005.07570](#) [hep-lat] [[Search inSPIRE](#)].
- [42] D. Kadoh, H. Oba, and S. Takeda, [arXiv:2107.08769](#) [cond-mat.str-el] [[Search inSPIRE](#)].
- [43] Y. Kuramashi and Y. Yoshimura, J. High Energy Phys. **04**, 089 (2020) [[arXiv:1911.06480](#) [hep-lat]] [[Search inSPIRE](#)].
- [44] J. Carlsson, [arXiv:0802.3409](#) [hep-lat] [[Search inSPIRE](#)].